Earth and Planetary Science Letters 291 (2010) 215–227

Contents lists available at ScienceDirect

Earth and Planetary Science Letters

journal homepage: www.elsevier.com/locate/epsl

A simple model of reaction-induced cracking applied to serpentinization and carbonation of peridotite

John F. Rudge [a,b,*], Peter B. Kelemen [b], Marc Spiegelman [b]

[a] Institute of Theoretical Geophysics, Bullard Laboratories, University of Cambridge, Madingley Road, Cambridge, CB3 0EZ, UK
[b] Lamont-Doherty Earth Observatory, Columbia University, Palisades, NY 10964, USA

ARTICLE INFO

Article history:
Received 8 July 2009
Received in revised form 6 November 2009
Accepted 8 January 2010
Available online 2 February 2010

Editor: Y. Ricard

Keywords:
weathering
carbon capture
reaction–diffusion
fracture mechanics

ABSTRACT

During chemical weathering there is the potential for a positive feedback process to occur: Chemical reactions cause volume changes, increasing stresses and potentially fracturing the rock. In turn, these fractures may enhance transport of chemicals through the rock, accelerating the weathering process. An idealised model of this feedback is presented. Simple scaling laws relate the speed of the weathering front to elastic properties, the rate of transport of reactants, and reaction rates. Five different regimes in the model are identified, although only two of these are appropriate for natural systems, where the reaction rate is a key control on the weathering rate. The model is applied to the carbonation and serpentinization of peridotite, chemical weathering processes which have potential industrial application in the storage of CO_2. If these weathering processes can be accelerated, CO_2 could be stored as carbonates in the peridotite in substantial quantities. This simple model suggests that it may be possible to boost the speed of the weathering front a millionfold by a combination of heating, increased partial pressure of CO_2, forced fluid flow, and hydrofracture.

1. Introduction

Chemical weathering is one of the most important processes that shapes the Earth's surface, and yet many aspects of it are still poorly understood. During weathering, a number of distinct physical processes occur, and these processes can interact with one another in interesting ways. Chemical weathering is driven by reactions between the rock and a mobile phase that moves through the rock, such as water, chemicals dissolved in water, or the air. As such the rate of chemical weathering is affected by how well this mobile phase can be transported through the rock, and by how fast it reacts with individual grains within the rock.

The reaction itself can influence the transport of the mobile phase in a variety of ways. One way in which it can do so is by the volume change (expansion or contraction) that can occur as a result of reaction. Volume change can cause increasing stress within the rock, and in turn these stresses can lead to fracturing of the rock, enhancing transport of the mobile phase and thus accelerating weathering (e.g. Correns and Steinborn, 1939; Correns, 1949; MacDonald and Fyfe, 1985; Walder and Hallet, 1985; Scherer, 1999, 2004; Rijniers et al., 2005; Fletcher et al., 2006; Malthe-Sørenssen et al., 2006; Flatt et al., 2007; Jamtveit et al., 2008).

The aim of this work is to develop a simple model of the physical processes involved in this particular feedback. To provide a concrete example of chemical weathering, we will discuss the application of the model to hydration and carbonation of peridotite, reactions between surface water and tectonically exposed mantle peridotite to form the hydrous mineral, serpentine, and Mg–Ca–carbonate minerals such as magnesite, dolomite and calcite. Serpentinization is best known as a process of alteration that happens near the seafloor, associated with hydrothermal circulation induced by mid-ocean ridge volcanism, but serpentinization and carbonation also occur via subaerial weathering (e.g. Barnes et al., 1967; Barnes and O'Neil, 1969; Neal and Stanger, 1985; Bruni et al., 2002). Weathering of peridotite is of current interest because of its potential for capture and storage of atmospheric CO_2 via mineral carbonation (Kelemen and Matter, 2008; Andreani et al., 2009). Also, serpentinization is an energy source for methanogenic organisms and is thought to be a possible substrate for the origin of life.

To make the presentation clearer, the main text describes the model formulation and key results, and detailed derivations are left to the appendices. The approach taken here is based on a simple model for the decomposition of solids developed by Yakobson (1991), which is reviewed in detail in Appendix D.1. The problem studied by Yakobson (1991) concerned the decomposition of one solid into another solid plus a mobile gas. The escape of the gas causes a volume decrease in the remaining solid which in turn causes fracturing. The fractures enable the gas to escape more readily and thus the rate of decomposition increases. The model presented here is also closely related to a model for spheroidal weathering (a type of chemical

* Corresponding author. Institute of Theoretical Geophysics, Bullard Laboratories, University of Cambridge, Madingley Road, Cambridge, CB3 0EZ, UK. Tel.: +44 1223 748938; fax: +44 1223 360779.
E-mail addresses: rudge@esc.cam.ac.uk (J.F. Rudge), peterk@ldeo.columbia.edu (P.B. Kelemen), mspieg@ldeo.columbia.edu (M. Spiegelman).

0012-821X/$ – see front matter © 2010 Elsevier B.V. All rights reserved.
doi:10.1016/j.epsl.2010.01.016

weathering) developed by Fletcher et al. (2006), and a detailed comparison of the two models can be found in Appendix D.2. The main difference between the model presented here over that of Fletcher et al. (2006) is that this model is analytically tractable, enabling a better understanding of different behaviours that can occur.

Unlike the decomposition problem of Yakobson (1991), which involves volume shrinkage, serpentinization, carbonation, and spheroidal weathering all involve volume expansion. Fluid–rock reactions that increase the solid volume, via reactions with host rock or precipitation of saturated minerals from the fluid, are often self-limiting because they fill porosity, reduce permeability, and create "reaction rims" of solid products that act as diffusive boundary layers between unreacted mineral reactants and fluid (e.g. Aharonov et al., 1998; Milsch et al., 2009; Morrow et al., 2001; Tenthorey et al., 1998). Decreasing permeability with reaction progress is commonly observed for hydration and carbonation of basalt (Alt and Teagle, 1999; Bartetzko, 2005; Becker and Davies, 2003; Schramm et al., 2005). On much shorter time and distance scales, experimental dissolution and carbonation of olivine commonly show a decrease in rate with time due to formation of a "passivating layer" of amorphous SiO_2 on olivine surfaces, after which the reaction rate is limited by diffusion through this solid layer (e.g. Chizmeshya et al., 2007).

However, it is also observed that precipitation of super-saturated minerals in pore space can fracture rocks, maintaining permeability and potentially exposing fresh mineral surfaces. For example, salts crystallizing from water in limestone and other building materials can fracture these materials, even while the fluid volume is decreasing (e.g. Scherer, 1999, 2004). Frost heaves and frost cracking are related phenomena (Walder and Hallet, 1985). Similarly, reaction between fluids and minerals that consume fluid components but increase the solid volume, such as hydration of solid lime (CaO) to produce portlandite ($Ca(OH)_2$), can cause polycrystalline rocks to fracture. Reaction-driven cracking has been observed experimentally in systems undergoing volume expansion, such as in the replacement of leucite by analcime (Jamtveit et al., 2009).

Extensive outcrops of serpentinite (completely hydrated peridotite) indicate that serpentinization is not always self-limiting. The ubiquitous presence of dense fracture networks in partially serpentinized peridotite, with fracture spacing ~50 μm, much smaller than the original olivine grain size, lends credence to the idea that serpentinization and cracking are coeval, as do the hierarchical nature of the fracture patterns (Iyer et al., 2008; Jamtveit et al., 2008). Without the presence of serpentine "glue" along these fracture networks, the host would be a powder, rather than a rock.

Similarly, the presence of extensive outcrops of listwanite (completely carbonated peridotite) in Oman (Neal and Stanger, 1985; Stanger, 1985; Wilde et al., 2002; Nasir et al., 2007) and elsewhere (e.g. Akbulut et al., 2006; Auclair et al., 1993; Hansen et al., 2005; Madu et al., 1990; Naldrett, 1966; Robinson et al., 2005; Santti et al., 2006; Schandl and Naldrett, 1992; Schandl and Wicks, 1993; Ucurum, 2000; Ucurum and Larson, 1999) demonstrates that olivine carbonation is not always self-limiting, despite increases in the solid volume. Listwanites have brecciated textures in outcrop and dense, hierarchical fracture networks extending to microscopic scales, filled by syn-kinematic carbonate and quartz veins, probably due to feedback between volume change, stress increase, and fracturing that maintains permeability and reactive surface area. Outcrop scale and microscopic relationships of carbonate veins in partially carbonated peridotites indicate coeval carbonate crystallization and formation of hierarchical crack networks, and volume expansion of the original host rock to accommodate carbonate precipitation. However, it may be that fracture filling by carbonates ultimately did limit reaction progress where we observe partially carbonated rocks. In the model that follows we assume the reaction-driven cracking is not self-limiting, although the negative feedbacks which could limit the process should be addressed in future work.

2. Model formulation

We consider a simple reaction whereby a mobile phase W (e.g. water or CO_2) reacts with an immobile solid A (e.g. peridotite) to form an immobile solid product B (e.g. serpentine or magnesite), $rW + sA \rightarrow B$ where r and s are the stoichiometric coefficients. The two solids A and B have different densities, and it is this difference in densities that causes stress to increase in the rock. We model the transport of the mobile phase W by simple diffusion, with an effective diffusivity D. The solid product B is produced at some rate Q which depends on the concentrations of the reagents W and A. Let w be the concentration of W (mol m^{-3}), a be the concentration of A, and b be the concentration of B. We describe the evolution of these concentrations by the following simple 1D advection–diffusion equations

$$\frac{\partial w}{\partial t} = D\frac{\partial^2 w}{\partial x^2} - rQ, \tag{1}$$

$$\frac{\partial a}{\partial t} = -sQ, \tag{2}$$

$$\frac{\partial b}{\partial t} = Q. \tag{3}$$

For simplicity, we assume a first order rate law for Q, namely

$$Q = kwa, \tag{4}$$

where k is a rate constant for the reaction (mol^{-1} m^3 s^{-1}).

We will assume that there exists a weathering front that propagates at some velocity v as a result of the reaction induced cracking (Fig. 1). Behind the front it is assumed that the rock has been cracked, that the stress has been relaxed, and that the mobile phase concentration is maintained at some fixed level w_0 (e.g. because it is in contact with a reservoir of the mobile phase and there is rapid flow through the cracked rock). Far ahead of the front it is assumed that there is no mobile phase, the rock is uncracked, and that there is only

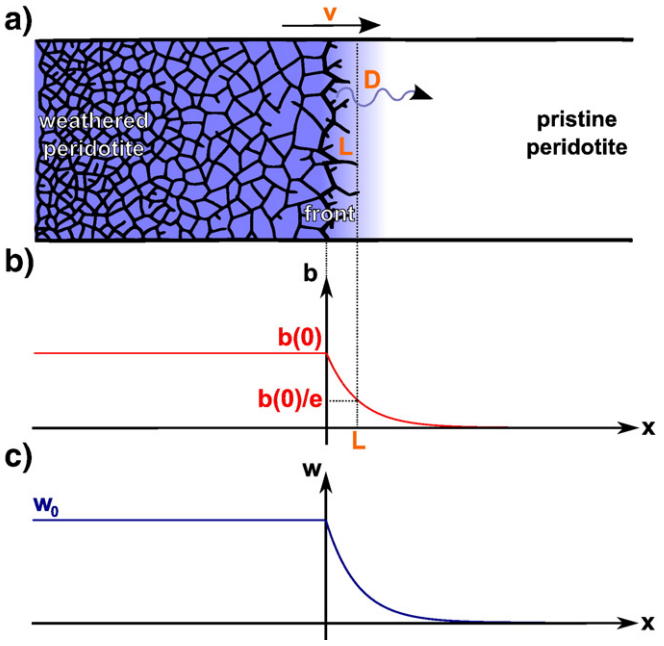

Fig. 1. Schematic diagram of the model. a) depicts the model geometry, with blue shading reflecting water concentration. b) and c) depict the concentration profiles of product b and mobile phase w respectively. The exact profiles depend on the choice of parameters; shown here are typical exponential profiles for regime 1.

the reactant solid A at some concentration a_0. The mobile phase diffuses into the uncracked rock, reacting as it goes.

In a frame moving with the front, the reaction–diffusion Eqs. (1)–(3) become

$$-v\frac{dw}{dx} = D\frac{d^2w}{dx^2} - rQ, \tag{5}$$

$$-v\frac{da}{dx} = -sQ, \tag{6}$$

$$-v\frac{db}{dx} = Q, \tag{7}$$

with boundary conditions

$$w(0) = w_0, \quad w(\infty) = 0, \tag{8}$$

$$a(\infty) = a_0, \tag{9}$$

$$b(\infty) = 0, \tag{10}$$

where $x=0$ is the position of the front in the moving frame and $x=\infty$ is a position far ahead of the weathering front. We will define $b_0 = a_0/s$, i.e. the concentration of solid B that would be produced if all of solid A were reacted. It is helpful also to define $\kappa = skw_0$, a rate constant (s^{-1}) for the production of solid B in the presence of a concentration w_0 of water. Note that Eqs. (6), (7), (9), and (10) imply that $a = s\,(b_0 - b)$, and thus we only need solve for w and b. The reaction rate Q is then given by Eq. (4) as

$$Q = \kappa\frac{w}{w_0}(b_0 - b), \tag{11}$$

where $\kappa = skw_0$.

As the reaction proceeds, stress builds up in the rock due to the volume change. We will assume production of B ahead of the front produces stresses σ in a simple linear fashion as

$$\sigma = \beta E b / b_0, \tag{12}$$

where E is the Young's modulus of the uncracked rock, and β is a non-dimensional prefactor that relates to the amount of volume change as

$$\beta = \frac{1}{3(1-\nu)}\frac{\Delta V}{V}. \tag{13}$$

Here ν is the Poisson's ratio, and $\Delta V/V$ is the relative volume change that occurs when all of solid A reacts to produce solid B.

Finally, we must relate the buildup of stress to the fracturing that drives the weathering front forward. We do this using a highly simplified fracture criterion, motivated by the linear fracture mechanics of a single crack. Suppose we have a crack of length L and apply a uniform stress σ over the crack faces. Then the crack will grow when the stress intensity factor K exceeds some critical value, known as the fracture toughness K_c (Pa $m^{1/2}$). To a first approximation, the stress intensity factor K is related to the applied stress and crack length through $K = \sigma L^{1/2}$. In detail there is a numerical prefactor that depends on the particular geometry and type of loading, but we shall not concern ourselves with this as our main interest is in overall scalings.

The rate of advance of the weathering front by fracturing should be determined by the stress field ahead of the front, $\sigma(x)$. To generate an appropriate fracture criterion we make three assumptions: Firstly, we assume a steadily propagating front, so that the cracks near the front are in a state of quasi-equilibrium and the stress intensity factor takes the critical value, $K = K_c$. Second, we hypothesise that the typical crack length L is determined by a typical length scale over which the stress field $\sigma(x)$ decays: formally, we let L be the length over which σ reaches 37% ($1/e$) of its value at the front. Finally, we assume that the value of σ at the front provides a good estimate for the loading on the cracks. Thus the fracture criterion we assume is

$$K_c = \sigma(0)L^{1/2}. \tag{14}$$

By combining Eqs. (12) and (14), the fracture criterion can be written as

$$K_c = \beta E L^{1/2} b(0)/b_0, \tag{15}$$

where the crack length L is chosen to be the length scale over which $b(x)$ decays (the value of x for which it reaches $1/e$ of its value at the front, Fig. 1b).

A fracture criterion, like that of Eq. (15), is necessary to close the equations and relate the reaction–diffusion problem to the fracturing. Similar criterion have been used in the models of Yakobson (1991) and Fletcher et al. (2006) (Appendix D). In the case of Yakobson's (1991) model, the stress intensity factor K is calculated for a single crack of length L subject to a loading $\sigma(x)$ on the crack faces, with K again assumed equal to the fracture toughness $K = K_c$. A dynamical hypothesis is made that the front propagates at its maximum possible velocity, and in order to do this it is found that the crack length scale L must be the length scale over which $\sigma(x)$ decays (up to some order 1 constants). In the model of Fletcher et al. (2006), the reaction ceases once the mobile phase concentration drops below a certain threshold, and the distance to this threshold determines the typical crack spacing. Thus the crack spacing in the model of Fletcher et al. (2006) is also set by a length scale in the reaction–diffusion problem, although this length scale is that of the mobile phase concentration profile rather than the product concentration profile. However, in many situations these length scales are the same (see Appendix D for further discussion). The fracture criterion of Fletcher et al. (2006) is written is terms of surface energy of fracture, and this can be directly related to the fracture toughness.

The above Eqs. (5)–(15) describe a simple model of a steadily propagating weathering front caused by volume changes due to reaction. The main aim of the analysis is to determine the front velocity v and the typical crack length L as a function of the given parameters.

3. Results

A detailed analysis of the equations above is presented in Appendices A to C, and we summarise the main results of the analysis in this section. The behaviour of the model is determined by just two non-dimensional parameters, Λ and Θ, defined by

$$\Lambda = \frac{\kappa}{D}\left(\frac{K_c}{\beta E}\right)^4, \quad \Theta = \frac{w_0}{rb_0}. \tag{16}$$

Λ relates the rate of reaction (κ), rate of transport (D), elastic properties (K_c and E), and volume change factor (β). Λ large means either rapid reaction, slow transport of mobile phase, tougher to fracture, or small volume changes. Θ is simply a concentration ratio, adjusted for stoichiometry. Large Θ simply means large amounts of mobile phase relative to solid.

The aim of the analysis is to find relationships for the weathering front velocity v and the characteristic crack length L. These can be expressed in terms of non-dimensional functions $\zeta(\Lambda, \Theta)$ and $\eta(\Lambda, \Theta)$ as

$$L = \left(\frac{K_c}{\beta E}\right)^2 \zeta(\Lambda, \Theta), \tag{17}$$

$$v = D\left(\frac{\beta E}{K_c}\right)^2 \eta(\Lambda, \Theta). \tag{18}$$

The length scale $(K_c/\beta E)^2$ is a natural length scale associated with fracture caused by volume change. In fact, this length scale provides a lower bound for L. $D(\beta E/K_c)^2$ provides a natural velocity scale.

The two non-dimensional functions $\eta(\Lambda, \Theta)$ and $\zeta(\Lambda, \Theta)$ have been calculated numerically for a range of Λ and Θ, and contour plots of the functions are shown in Figs. 2 and 3. The main features of these plots are straightforward to understand when we interpret Λ as a non-dimensional reaction rate and Θ as a non-dimensional water concentration. Non-dimensional front velocity $\eta(\Lambda, \Theta)$ increases with increasing Λ and increasing Θ, which reflects the fact that the weathering front moves faster if the reaction happens faster or if there is more water present. Non-dimensional crack length $\zeta(\Lambda, \Theta)$ increases with decreasing Λ, which reflects the fact that we get longer cracks with slower reactions (since slower reactions allow more time for the water to diffuse further past the front). $\zeta(\Lambda, \Theta)$ also increases with increasing Θ, as more water present also allows transport further past the front.

While the functions $\eta(\Lambda, \Theta)$ and $\zeta(\Lambda, \Theta)$ can be calculated numerically, it will often be the case that the non-dimensional parameters Λ and Θ are large or small. In such cases, there are some simple analytical expressions for the forms of $\eta(\Lambda, \Theta)$ and $\zeta(\Lambda, \Theta)$, and the corresponding dimensional expressions for v and L are shown in Table 1. Based on the relative magnitudes of Λ and Θ, the parameter space divides into five asymptotic regimes as shown in Fig. 4.

Some aspects of the asymptotic regimes have clear physical interpretations. For example, regimes 4 and 5 represent very rapid reaction, and the corresponding results are independent of the rate constant κ. In these regimes all the solid reactant is used up, and the fracture scale reaches its lower limit (known as "brittle fracturing"). In regime 3 there is weak (logarithmic) dependence on the reaction rate κ, but the fracture scale is still that of brittle fracturing and all the solid reactant is still used up. In regimes 1 and 2 the reaction is slow and limits the speed at which the front can propagate ("reaction controlled"). The front velocity still depends on the elastic properties and the diffusivity of the mobile phase, but more weakly. The corresponding fracture scales are larger, and in regime 1, the crack length L is completely independent of the elastic properties. The difference between regimes 1 and 2 is best understood in terms of the dependence on Θ: In regime1, Θ is small and propagation of the front is limited by the availability of water. Regime 2 has larger Θ and front propagation is no longer controlled by the availability of water as it is plentiful, and this is reflected in the expressions for v and L which are independent of Θ. Similarly, the expressions in regime 3 are independent of Θ, and the transition from regime 3 to regime 4 reflects the point at which the availability of water again becomes a controlling factor.

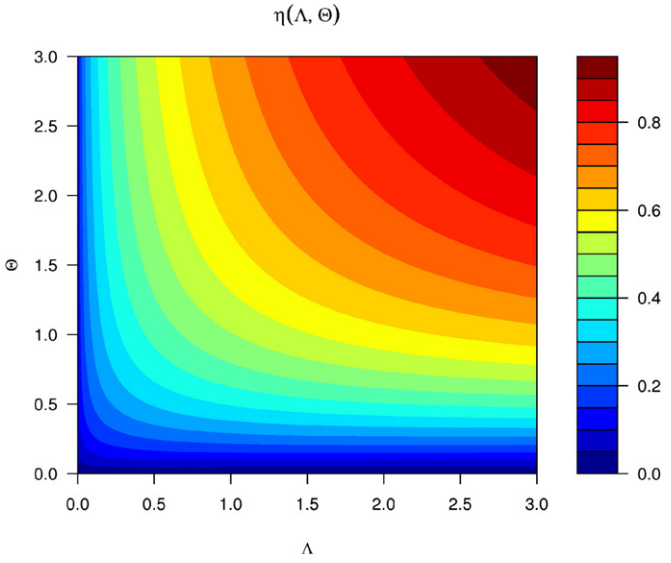

Fig. 2. Results of numerical solutions showing $\eta = (v/D)(K_c/\beta E)^2$ (a non-dimensional front velocity) as a function of Λ and Θ.

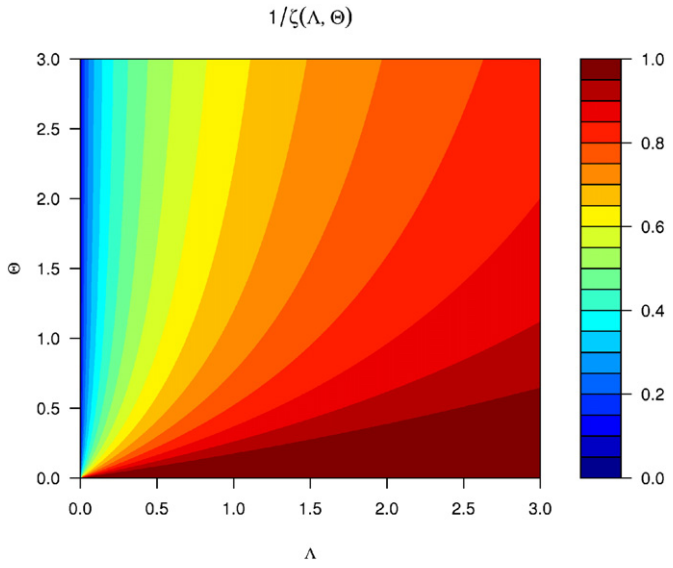

Fig. 3. Results of numerical solutions showing $1/\zeta$ as a function of Λ and Θ. $\zeta = L(\beta E/K_c)^2$ is a non-dimensional crack length. It is more convenient to plot $1/\zeta$ rather than ζ due to the singular behaviour of ζ near $\Lambda = 0$.

4. Serpentinization and carbonation of peridotite

The model may be useful in understanding some of the controls on the rate of serpentinization and carbonation of peridotite during weathering. In turn, this understanding could be valuable in designing systems for enhanced, in situ carbonation of peridotite for CO_2 capture and storage. Unfortunately, a number of the model parameters are not well known, notably the rate of transport of water (D), and this makes applying the model to real situations difficult. However, some useful order of magnitude estimates can be made.

The elastic properties of peridotite are fairly well known, with a Young's modulus $E \sim 10^{11}$ Pa and fracture toughness $K_c \sim 10^6$ Pa m$^{1/2}$. A typical volume expansion is around 20%, leading to $\beta \sim 0.13$ for a Poisson's ratio $\nu \sim 0.25$. The reaction rate κ can be estimated from experimental data. Though experiments are done on powder, inferences can be made on the reactive surface area in powder versus the grain size in a rock that allows scaling of the experimental data to a natural situation. The parameterisations of carbonation and serpentinization rate used are those of Kelemen and Matter (2008).

Table 1
A summary of the asymptotic regimes for the model in dimensional units. Here $W(z)$ is the Lambert function (the solution of $z = W(z)\exp(W(z))$).

Regime	Range of validity	v	L
1	$\Theta^5 \ll \Lambda \ll \Theta$	$\frac{\beta E}{K_c}\kappa^{1/4}(D\Theta)^{3/4}$	$\left(\frac{D\Theta}{\kappa}\right)^{1/2}$
2	$\Lambda \ll 1$, $\Lambda \ll \Theta^5$	$D^{3/5}\left(\frac{\beta E\kappa}{K_c}\right)^{2/5}$	$\left(\frac{K_c D}{\beta E\kappa}\right)^{2/5}$
3	$1 \ll \Lambda \ll \Theta(\log\Theta)^2$	$2D\left(\frac{\beta E}{K_c}\right)^2 W\left(\frac{1}{2}\left(\frac{K_c}{\beta E}\right)^2\left(\frac{\kappa}{D}\right)^{1/2}\right)$	$\left(\frac{K_c}{\beta E}\right)^2$
4	$1 \ll \Theta$, $\Theta(\log\Theta)^2 \ll \Lambda$	$D\left(\frac{\beta E}{K_c}\right)^2 \log\Theta$	$\left(\frac{K_c}{\beta E}\right)^2$
5	$\Theta \ll 1$, $\Theta \ll \Lambda$	$D\left(\frac{\beta E}{K_c}\right)^2 \Theta$	$\left(\frac{K_c}{\beta E}\right)^2$

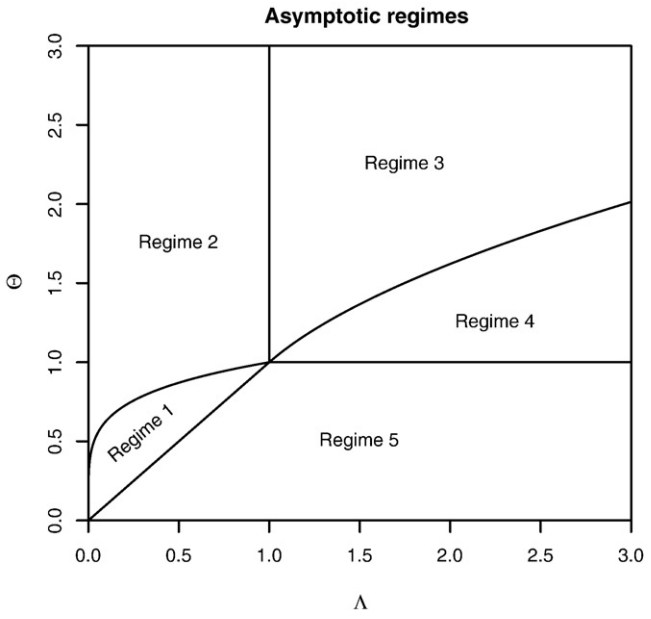

Fig. 4. A map of the asymptotic regimes in terms of Λ and Θ.

For serpentinization, the experimental data of Martin and Fyfe (1970) was parameterised as

$$\kappa_{\text{serp.}} = \kappa_0 \left(\frac{a_0}{a}\right)^2 e^{-\alpha(T-T_0)^2}, \tag{19}$$

where $\kappa_0 = 10^{-6}\,\text{s}^{-1}$, $a_0 = 70\,\mu\text{m}$, $\alpha = 2.09\times10^{-4}\,^\circ\text{C}^{-2}$, $T_0 = 260\,^\circ\text{C}$. The experiments were performed with 70 μm grains, and the factor $(a_0/a)^2$ reflects the scaling due to surface area effects, where a is the typical grain size controlling the reaction. T_0 is the temperature at which the serpentinization rate reaches its peak, and κ_0 is the corresponding peak rate for 70 μm grains.

For carbonation, the experimental data of O'Connor et al. (2005) was parameterised as

$$\kappa_{\text{carb.}} = \kappa_0 \left(\frac{a_0}{a}\right)^2 \left(\frac{P_{CO_2}}{P_0}\right)^{1/2} e^{-\alpha(T-T_0)^2}, \tag{20}$$

where $\kappa_0 = 1.15\times10^{-5}\,\text{s}^{-1}$, $a_0 = 70\,\mu\text{m}$, $P_0 = 1$ bar, $\alpha = 3.34\times10^{-4}\,^\circ\text{C}^{-2}$, $T_0 = 185\,^\circ\text{C}$. There is an additional influence on the carbonation rate due to the partial pressure P_{CO_2} of carbon dioxide. Here, κ_0 is the peak reaction rate at a reference partial pressure P_0 of 1 bar, again with 70 μm grains.

Typical summer temperatures in Oman are around $T \sim 50\,^\circ\text{C}$. Typical grain sizes of peridotite are around $a \sim 0.1$ mm, and a similar value is obtained for estimates of crack spacing in crystalline rocks that are roughly similar to peridotite (Sprunt and Brace, 1974; Brace, 1977; Wong et al., 1989). Typical partial pressures are around $P_{CO_2} \sim 4\times10^{-4}$ bar. Thus estimated natural reaction rates are $\kappa_{\text{serp.}} \sim 5\times10^{-11}\,\text{s}^{-1}$ for serpentinization, and $\kappa_{\text{carb.}} \sim 2.5\times10^{-10}\,\text{s}^{-1}$ for carbonation.

The speed of the weathering front in the Oman ophiolite has been estimated at $v \sim 0.3\,\text{mm yr}^{-1}$ (Poupeau et al., 1998), which is in keeping with the observation that the average ^{14}C age of carbonate veins in peridotite exposed to weathering in Oman, in a weathering horizon ~10 m thick, is about 26,000 yr (Kelemen and Matter, 2008).

Assuming asymptotic regime 1, the expressions for v and L are (Table 1)

$$v = \frac{\beta E}{K_c}\kappa^{1/4}(D\Theta)^{3/4}, \quad L = \left(\frac{D\Theta}{\kappa}\right)^{1/2}, \tag{21}$$

which are valid provided

$$\Theta^4 \ll \frac{\Lambda}{\Theta} \ll 1, \tag{22}$$

which has to be checked. Since we have a reasonable estimate for v, the above equations can be rearranged to provide expressions for the effective diffusivity D required to match the observed weathering rate,

$$D\Theta = \left(\frac{K_c v}{\beta E}\right)^{4/3} \kappa^{-1/3}, \tag{23}$$

and corresponding expressions for L and Λ/Θ are

$$L = \left(\frac{K_c v}{\beta E \kappa}\right)^{2/3}, \quad \frac{\Lambda}{\Theta} = \frac{\kappa}{D\Theta}\left(\frac{K_c}{\beta E}\right)^4. \tag{24}$$

Using the carbonation rate $\kappa_{\text{carb.}}$, the estimates above imply $D\Theta \sim 10^{-17}\,\text{m}^2\,\text{s}^{-1}$ and a typical crack length scale $L \sim 0.2$ mm (very similar to the proposed grain size $a \sim 0.1$ mm). $\Lambda/\Theta = 8\times10^{-10}$ which is certainly much less than 1 (as required by Eq. (22)), and will be greater than Θ^4, provided $\Theta < 0.005$. Since the estimates above are only weakly dependent on κ (dependences of $\kappa^{-1/3}$ and $\kappa^{-2/3}$), using the serpentinization rate $\kappa_{\text{serp.}}$ instead (with its factor of 5 slower rate), produces fairly similar estimates.

Θ represents a ratio of mobile phase concentration to solid reactant concentration, which can be estimated based on the amount of water that can be stored on grain boundaries or microcracks in the rock. Laboratory-based estimates of grain boundary width in crystalline rocks are around $w \sim 0.01\,\mu\text{m}$ (Farver and Yund, 1991, 1992; Yund, 1997), which provide estimates of porosity $\phi \sim 3w/a = 3\times10^{-4}$. Taking this porosity ϕ as an estimate for Θ yields an effective diffusivity $D \sim 3\times10^{-14}\,\text{m}^2\,\text{s}^{-1}$ using Eq. (23). The effective diffusivity D encompasses a number of different processes that cause the mobile phase to be transported through the rock, including advection, diffusion, and dispersion, and is a difficult quantity to estimate directly. However, the required value of D is fairly similar to that expected from experimental measurements of diffusion of water-in-water $D_{\text{water-in-water}} \sim 6\times10^{-11}\,\text{m}^2\,\text{s}^{-1}$ (Farver and Yund, 1992, extrapolated to 50 °C), which when multiplied by ϕ gives an effective diffusivity $D \sim 2\times10^{-14}\,\text{m}^2\,\text{s}^{-1}$, very close to the required value.

For practical industrial storage of CO_2 we would like to increase the front velocity v,

$$v = \frac{\beta E}{K_c}\kappa^{1/4}(D\Theta)^{3/4}, \tag{25}$$

by many orders of magnitude. To do this we can either increase the reaction rate (κ), increase the transport of mobile phase (D), or increase the availability of mobile phase (Θ). It is possible to estimate the order of magnitude increases in front velocity one can expect under different engineered conditions. One of the simplest ways of accelerating the weathering process is by heating: at the optimal temperature for carbonation (185 °C), the rate of carbonation is 450 times greater than it is at 50 °C. However, since the front velocity depends only weakly on κ, this leads to only a 5 fold increase in front velocity. Temperature will also influence the effective diffusivity of the mobile phase. Based on the temperature dependence of water-in-water diffusion of (Farver and Yund, 1992), this could be expected to increase D by around a factor of 5, which leads to another 3 fold increase in v. Hence heating overall could potentially lead to a 15 times greater front velocity. Such heating may be self sustaining due to the exothermic nature of the serpentinization and carbonation reactions (Kelemen and Matter, 2008).

The kinetics of carbonation is very dependent on the partial pressure of CO_2, and increasing this is another way to speed the front.

An increase in P_{CO_2} to 300 bar would lead to a 900 fold increase in the carbonation rate, and a corresponding 5 fold increase in front velocity. Thus heating and elevated partial pressure combined could lead to a 75 times faster front velocity, which is still somewhat short of what one would like for industrial applications.

According to Eq. (25), the effective diffusivity D (which describes the transport of the mobile phase through the rock), and Θ (which describes the availability of water) have a much greater influence on the front velocity than κ (the reaction rate). $D\Theta$ will need to be increased by orders of magnitude to produce industrially viable solutions. One way of doing this is by increasing the porosity, which could be done by hydrofracturing the rock at depth. An increase in porosity to 1% (typical for cracked rock, e.g. (Wu et al., 2006)) could be expected to produce a 200 fold increase in front velocity.

However, even larger effective diffusivities may be possible if the flow is forced by applying a pressure gradient. Rapid fluid flow within the fractures will cause enhanced concentration gradients and thus increase the effective diffusivity. A rough estimate of the effective diffusivity for forced flow in cracked rock is $D \approx \phi v_{\text{crack}} \alpha$ where ϕ is the porosity, v_{crack} is the fluid velocity in the crack, and α is a dispersivity parameter (Wu et al., 2010). Darcy velocities $\phi v_{\text{crack}} \sim 10^{-4}\,\text{m s}^{-1}$ can be generated with moderate pressure gradients (a typical permeability of cracked rock is $k \sim 10^{-12}\,\text{m}^2$, (Wu et al., 2006)), and a crude estimate of the dispersivity parameter can be obtained from a typical crack width, $\alpha \sim 2\times10^{-5}$ m. These estimates lead to effective diffusivities $D \sim 2\times10^{-9}\,\text{m}^2\,\text{s}^{-1}$, 70,000 larger than the inferred natural effective diffusivity, and producing a 4,000 fold increase in front velocity. With a combination of all the above suggestions, it may be possible to go from the natural weathering rate of tenths of millimetres a year to an industrial rate of hundreds of metres a year.

In estimating the front velocities under engineered circumstances, it was assumed that regime 1 held throughout (Eq. (25) was used), and this assumption should be checked. The natural estimates have $\Lambda \sim 2\times10^{-13}$. The largest Λ in the engineered circumstances is when the reaction rate κ alone is increased (see Eq. (16)). An increase in κ by a factor of 4×10^5 (i.e. heating and increased partial pressure) gives $\Lambda \sim 8\times10^{-8}$. This value of Λ certainly satisfies $\Lambda \ll 1$ and $\Lambda \ll \Theta$ for any reasonable value of Θ, and hence only regimes 1 or 2 are ever appropriate (Table 1). If $\Theta^5 \ll \Lambda$ we are in regime 1; if $\Theta^5 \gg \Lambda$ we are in regime 2. In the natural situation, it was estimated that $\Theta \sim 3\times10^{-4}$ and thus $\Theta^5 \sim 2\times10^{-18}$, and regime 1 is appropriate. However, in the engineered situations where porosity is increased $\Theta \sim 0.01$ and thus $\Theta^5 \sim 10^{-10}$, which is greater than Λ in some scenarios. Hence regime 2 is a possibility in some engineered conditions, where water is plentiful and the front velocity v becomes independent of Θ. However, the velocities estimated by the regime 1 and 2 equations differ by only $(\Lambda/\Theta^5)^{3/20}$, which at most a factor of 2 for the scenarios in which regime 2 expressions are appropriate, so this does not change the results greatly.

In oceanic settings, rates of serpentinization are very poorly known. One pertinent observation is that peridotites exposed on the seafloor at and near mid-ocean ridges are invariably, partially to completely serpentinized. No significant gradient in the degree of serpentinization is observed as a function of depth in drill holes extending for 100 to 200 m (Bach et al., 2004; Kelemen et al., 2004; Paulick et al., 2006; Kelemen et al., 2007). Tectonically induced faults and shear zones are common in this environment. Once formed, these features could enhance the rate of serpentinization in peridotites near the seafloor, yet they have nothing to do with reaction-induced cracking. However, seismic data suggest a gradient of decreasing serpentinization that extends downward from the seafloor over ~5 km in some places (Fig. F5, Chapter 1, (Kelemen et al., 2004)). The presence of such a gradient suggests generally continuous, downward transport of water through a fracture network, rather than localized transport along a few large faults. Though these and other, similar observations were made at slow-spreading ridges, where rates of uplift and tectonic denudation are slow, at least some of the peridotites exposed on the seafloor must have approached the seafloor within the past 10^6 yr, if not less. Thus a minimum rate for propagation of a serpentinization front in oceanic crust might be $v \sim 5\,\text{mm yr}^{-1}$ (around a factor of 10 faster than the Oman weathering rate), and the actual rates could be orders of magnitude faster. Applying the model in this setting, with a kinetic rate $\kappa_{\text{serp.}} \sim 5\times10^{-11}\,\text{s}^{-1}$, implies lower bounds of $D\Theta \sim 8\times10^{-16}\,\text{m}^2\,\text{s}^{-1}$ and $L \sim 0.4$ mm, very similar to the values calculated for Oman peridotite weathering, although these values could be much larger if the front velocities are orders of magnitude faster.

5. Conclusion

The main results of this work are presented in Table 1, which show how the speed and morphology of a chemical weathering front depends on the rate of reaction, rate of fluid transport, elastic properties, and amount of volume change, within the framework of a highly idealised model. For realistic parameter values, only regimes 1 and 2 will be observed ("reaction controlled regimes"). The model predicts the velocity of a reaction-driven cracking front in rocks undergoing volume change due to fluid-rock interaction, and the simple scalings that result are the first step towards understanding the behaviour of more sophisticated models. There are many avenues for future work on this problem. It would be very useful to look further at 2D problems (e.g. Malthe-Sørenssen et al., 2006; Røyne et al., 2008), where the elastic stress field and its boundary conditions can be modelled more carefully, and a better treatment of the fracture criterion could then be attempted. As mentioned in the introduction, there are potential negative feedbacks that may limit the reaction-driven cracking which are not included in this model, and should be explored in the future. Notably, the volume expanding reaction may clog the pore space and hinder transport of the mobile phase rather than aiding transport by fracturing (e.g. Andreani et al., 2009). This feedback may be possible to study in a 1D model using an evolution equation for permeability: work on this is ongoing.

Acknowledgements

We thank the editor Yanick Ricard and three anonymous reviewers for their valuable comments. We also thank David Bercovici for many useful discussions. This work was supported by NSF grants OCE-0452457 and EAR-0610138.

Appendix A. Non-dimensionalisation

The problem has just two non-dimensional parameters, Λ and Θ, defined by

$$\Lambda = \frac{\kappa}{D}\left(\frac{K_c}{\beta E}\right)^4, \quad \Theta = \frac{w_0}{r b_0}. \tag{26}$$

In presenting the final results, it is convenient to non-dimensionalise on the natural length scale that arises in the fracture criterion (15), namely $(K_c/\beta E)^2$. Non-dimensional front velocities and crack lengths can be defined using this length scale as

$$\eta = \frac{v}{D}\left(\frac{K_c}{\beta E}\right)^2, \quad \zeta = L\left(\frac{\beta E}{K_c}\right)^2. \tag{27}$$

Non-dimensionally, the aim of the analysis is to find $\eta(\Lambda, \Theta)$ and $\zeta(\Lambda, \Theta)$. The fracture criterion (15) takes the simple form

$$1 = \zeta^{1/2} b'(0), \tag{28}$$

where $b' = b/b_0$ is a rescaled concentration.

While non-dimensionalising on $(K_c/\beta E)^2$ is convenient for the final results and the fracture criterion, it is cumbersome for reaction–diffusion part of the problem, as that problem does not directly contain the elastic parameters. A more convenient length scale for the reaction–diffusion problem is D/v, and we introduce non-dimensional variables γ and λ as

$$\gamma = \frac{D\kappa}{v^2} = \frac{\Lambda}{\eta^2}, \quad \lambda = \frac{vL}{D} = \eta\zeta. \tag{29}$$

Introducing a rescaled concentration $w' = w/w_0$, a rescaled reaction rate $Q' = Q/\kappa b_0$, and a non-dimensional co-ordinate $x' = xv/D$, the reaction–diffusion problem becomes

$$-\frac{dw'}{dx'} = \frac{d^2w'}{dx'^2} - \frac{\gamma}{\Theta}Q', \tag{30}$$

$$-\frac{db'}{dx'} = \gamma Q', \tag{31}$$

$$w'(0) = 1, \quad w'(\infty) = 0, \tag{32}$$

$$b'(\infty) = 0, \tag{33}$$

$$Q' = w'(1-b'). \tag{34}$$

The strategy for solution of the above equations is as follows: The reaction–diffusion problem (Eqs. (30)–(34)) determines $\lambda(\gamma, \Theta)$ and $b'(0; \gamma, \Theta)$ where $\lambda(\gamma, \Theta)$ is the non-dimensional length scale over which $b'(x'; \gamma, \Theta)$ decays, and $b'(0; \gamma, \Theta)$ is the value of $b'(x'; \gamma, \Theta)$ at the front. The relationships between the different non-dimensional parameters (29) and the non-dimensional fracture criterion (28) can then be used to find $\eta(\Lambda, \Theta)$ and $\zeta(\Lambda, \Theta)$.

B. The reaction–diffusion problem

From now on, we will drop primes and work solely with non-dimensional variables. The reaction–diffusion system (Eqs. (30)–(34)) can be integrated once to give

$$\frac{dw}{dx} = -w - \frac{1}{\Theta}b, \tag{35}$$

$$\frac{db}{dx} = -\gamma Q = -\gamma w(1-b), \tag{36}$$

with boundary conditions

$$w(0) = 1, \quad w(\infty) = 0. \tag{37}$$

This is a second order non-linear two-point boundary value problem. For the connection with the fracture mechanics problem, we want to find $\lambda = \lambda(\gamma, \Theta)$ (the length scale over which b decays) and $b(0) = b(0; \gamma, \Theta)$ (the magnitude of b at the front). For moderate values of γ and Θ the above problem is easy to solve numerically. For very large or very small values of γ and Θ numerical solutions are more difficult. However, in these cases asymptotic solutions provide a very good approximation.

Numerical solutions showing typical concentration profiles are shown in Fig. 5. From such profiles it is straightforward to calculate λ and $b(0)$. Shown in Figs. 6 and 7 are contour plots showing the behaviour of λ and $b(0)$ as a function of γ and Θ.

B.1. Asymptotic solutions

There are a number of simple asymptotic approximations to the governing equations valid in certain parameter regimes. They provide simple analytic expressions for λ and $b(0)$ in the relevant regimes.

B.1.1. Linearisation: regimes 1 and 2

The simplest asymptotic solution arises when we linearise the governing equations, namely

$$\frac{dw}{dx} = -w - \frac{1}{\Theta}b, \tag{38}$$

$$\frac{db}{dx} = -\gamma w. \tag{39}$$

Such an approximation will be justified provided $b \ll 1$. The above equations are easily integrated to give

$$w = e^{-mx}, \quad b = \frac{\gamma}{m}e^{-mx}, \tag{40}$$

where

$$m = \frac{-1 + \sqrt{1 + 4\gamma/\Theta}}{2}. \tag{41}$$

Hence

$$\lambda = \frac{1}{m}, \quad b(0) = \frac{\gamma}{m}. \tag{42}$$

These expressions can be further simplified if we assume either $\gamma \gg \Theta$ or $\gamma \ll \Theta$. Call $\gamma \gg \Theta$ regime 1, and $\gamma \ll \Theta$ regime 2. In regime 1 we have $m \sim (\gamma/\Theta)^{1/2}$ and

$$w = e^{-x(\gamma/\Theta)^{1/2}}, \quad b = (\gamma\Theta)^{1/2}e^{-x(\gamma/\Theta)^{1/2}}, \tag{43}$$

$$\lambda = \left(\frac{\Theta}{\gamma}\right)^{1/2}, \quad b(0) = (\gamma\Theta)^{1/2}. \tag{44}$$

Consistency of the approximation ($b \ll 1$) implies that regime 1 is the region where $\Theta \ll \gamma \ll \Theta^{-1}$.

In regime 2 we have $m \sim 1$ and

$$w = e^{-x}, \quad b = \gamma e^{-x}, \tag{45}$$

$$\lambda = 1, \quad b(0) = \gamma. \tag{46}$$

Consistency ($b \ll 1$) implies that regime 2 is the region where $\gamma \ll 1$ and $\gamma \gg \Theta$.

B.1.2. Regime 3

Another approximation to the governing equations that can be integrated analytically is

$$\frac{dw}{dx} = -w, \tag{47}$$

$$\frac{db}{dx} = -\gamma w(1-b), \tag{48}$$

and will be valid provided $b \ll \Theta w$. The solution is

$$w = e^{-x}, \tag{49}$$

$$b = 1 - \exp\left(-\gamma e^{-x}\right). \tag{50}$$

If $\gamma \ll 1$ then this reduces to regime 2, where $b = \gamma e^{-x}$. Assume the opposite here, $\gamma \gg 1$. Then

$$\lambda = \log\gamma, \tag{51}$$

$$b(0) = 1. \tag{52}$$

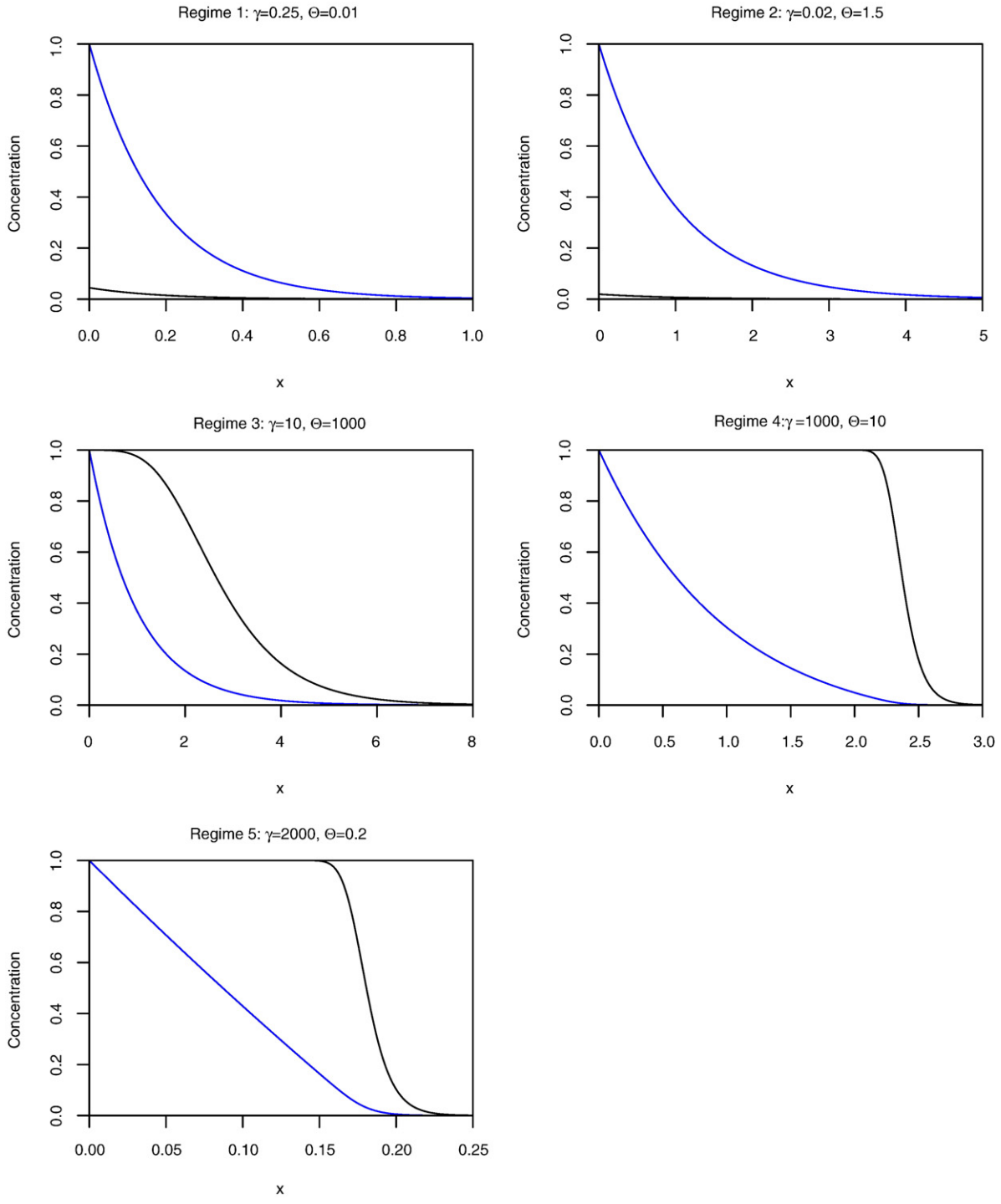

Fig. 5. Numerical solutions of the non-dimensional reaction–diffusion equation. Parameters have been chosen to give examples of the different asymptotic regimes. Blue curves are the mobile phase w, black curves are the immobile product b.

With this approximation the concentration profile for b has a boundary layer structure, where $b \sim 1$ until $x \sim \lambda$. The boundary layer thickness is order 1. Consistency ($b \ll \Theta w$) implies that regime 3 is the region where $1 \ll \gamma \ll \Theta$.

B.1.3. Regime 5

Consider the approximate set of equations

$$\frac{dw}{dx} = -\frac{1}{\Theta} b, \tag{53}$$

$$\frac{db}{dx} = -\gamma w(1-b), \tag{54}$$

which are valid if $\Theta w \ll b$. If $\gamma\Theta \ll 1$ this reduces to regime 1. Assume the opposite here, that $\gamma\Theta \gg 1$. The above can be combined to give

$$\frac{\Theta}{\gamma}\frac{d^2w}{dx^2} - \Theta w \frac{dw}{dx} - w = 0. \tag{55}$$

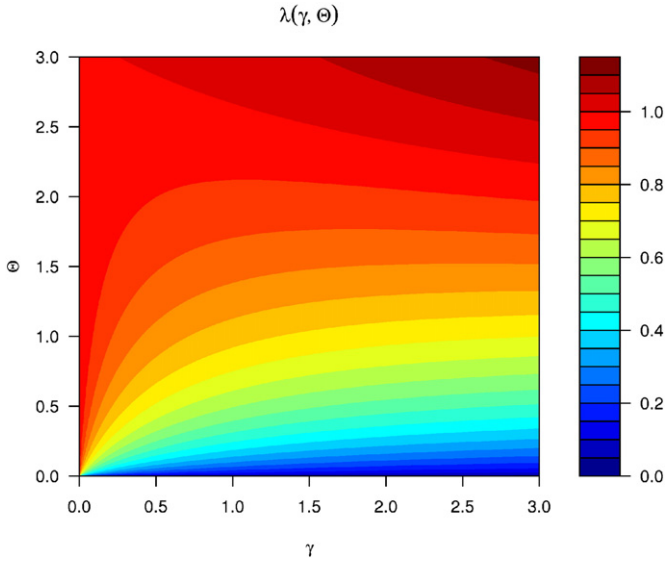

Fig. 6. Results of numerical solutions showing $\lambda = Lv/D$ as a function of γ and Θ.

It is helpful to introduce a rescaled co-ordinate $y = x/\Theta$,

$$\frac{1}{\gamma\Theta}\frac{d^2w}{dy^2} - w\frac{dw}{dy} - w = 0. \tag{56}$$

$\gamma\Theta \gg 1$ is a singular perturbation of the above equation. In this case, the solution has the approximate form

$$w = \begin{cases} 1 - x/\Theta, & x < \Theta, \\ 0, & x > \Theta. \end{cases} \tag{57}$$

$$b = \begin{cases} 1, & x < \Theta, \\ 0, & x > \Theta. \end{cases} \tag{58}$$

Thus

$$\lambda = \Theta, \quad b(0) = 1. \tag{59}$$

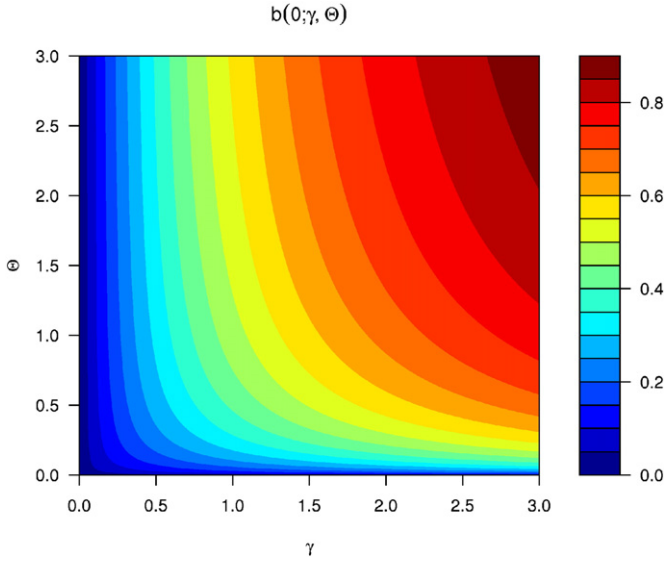

Fig. 7. Results of numerical solutions showing $b(0)$ as a function of γ and Θ.

In detail, there is a boundary layer in the solution at $x = \lambda$, with a thickness of order $(\Theta/\gamma)^{1/2}$. Consistency ($\Theta w \ll b$) implies that regime 5 is the region where $\gamma^{-1} \ll \Theta \ll 1$.

B.1.4. Regime 4

The remaining unexplored parameter regime has $1 \ll \Theta \ll \gamma$. We again expect a boundary layer behaviour. However, in this regime both terms in Eq. (35) are important. Consider Eq. (35) with $b = 1$,

$$\frac{dw}{dx} = -w - \frac{1}{\Theta}, \tag{60}$$

which has solution

$$w = \left(1 + \frac{1}{\Theta}\right)e^{-x} - \frac{1}{\Theta}. \tag{61}$$

This is zero when $x = \log(1+\Theta)$, and this is where the boundary layer for b is expected. If $\Theta \ll 1$ this returns to regime 5, whereas if $\Theta \gg 1$ we have

$$\lambda = \log\Theta, \quad b(0) = 1. \tag{62}$$

The initial balance of terms has $\Theta w \gg b$ as in regime 3, but for $x \gg 1$ we have $\Theta w \ll b$ as in regime 5. The boundary layer structure at $x = \lambda$ should be similar to regime 4, with an order $(\Theta/\gamma)^{1/2}$ thickness.

Table 2 summarises the different asymptotic regimes for the reaction–diffusion problem, and a regime diagram is shown in Fig. 8.

C. The fracture criterion

Once $\lambda(\gamma, \Theta)$ and $b(0; \gamma, \Theta)$ are known, all that remains is the fracture criterion (28),

$$1 = \zeta^{1/2} b(0), \tag{63}$$

and the additional relationships (29)

$$\gamma = \Lambda/\eta^2, \quad \zeta = \lambda/\eta. \tag{64}$$

These can be combined to give

$$1 = \left(\frac{\lambda\left(\Lambda/\eta^2, \Theta\right)}{\eta}\right)^{1/2} b\left(0; \Lambda/\eta^2, \Theta\right), \tag{65}$$

which is an expression that can be inverted to find $\eta(\Lambda, \Theta)$. Moreover, the fracture criterion (63) can be rewritten as

$$\zeta = \left(b(0, \Lambda/\eta^2, \Theta)\right)^{-2}, \tag{66}$$

and thus we can find $\zeta(\Lambda, \Theta)$ given $\eta(\Lambda, \Theta)$. This completes the problem; numerical solutions are shown in Figs. 2 and 3. Asymptotic solutions are given in Table 3, with a regime diagram in Fig. 4. The final dimensional results are given in Table 1.

Table 2
A summary of the asymptotic regimes for the reaction–diffusion problem.

Regime	Range of validity	λ	$b(0)$
1	$\Theta \ll \gamma \ll \Theta^{-1}$	$\Theta^{1/2}\gamma^{-1/2}$	$\Theta^{1/2}\gamma^{1/2}$
2	$\gamma \ll 1, \gamma \ll \Theta$	1	γ
3	$1 \ll \gamma \ll \Theta$	$\log\gamma$	1
4	$1 \ll \Theta \ll \gamma$	$\log\Theta$	1
5	$\gamma^{-1} \ll \Theta \ll 1$	Θ	1

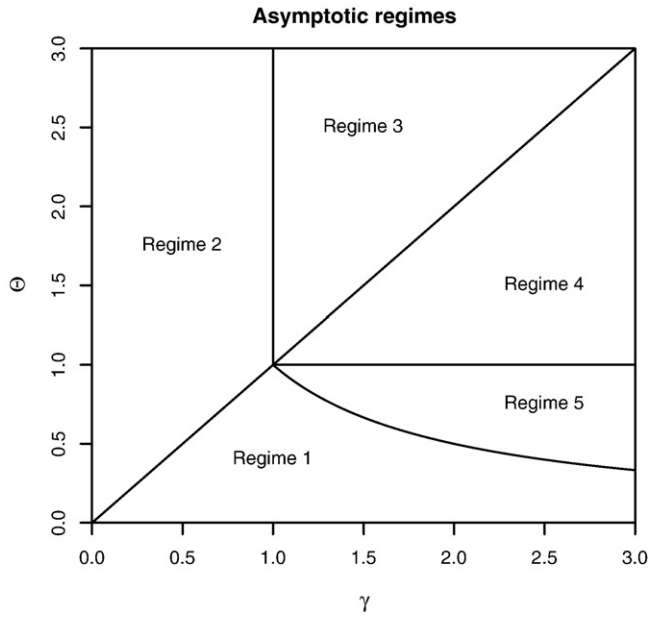

Fig. 8. A map of the asymptotic regimes for the reaction–diffusion problem in terms of γ and Θ.

D. Related problems

D.1. Decomposition of solids: Yakobson (1991)

In this work we have used a very simple fracture criterion, given in dimensional form by

$$K_c = \sigma(0)L^{1/2}, \tag{67}$$

where the crack length L was chosen to be length scale δ over which $\sigma(x)$ decays.

Similar results can be obtained from other fracture criterion. For example, in the model of decomposition of solids by (Yakobson, 1991), the following fracture criterion was used

$$K_c = 2\left(\frac{L}{\pi}\right)^{1/2}\int_0^L \frac{\sigma(x)}{(L^2-x^2)^{1/2}}dx. \tag{68}$$

As it stands, the above equation produces a family of solutions relating v to L. In Yakobson's (1991) model, the final choice of L is made by a dynamical hypothesis that assumes v takes its maximum value. In fact, Yakobson's (1991) criterion can be related to the simple one used here. Let us suppose that $\sigma(x)$ can be written as

$$\sigma(x) = \sigma(0)g(x/\delta), \tag{69}$$

Table 3
A summary of the asymptotic regimes for the full problem. Here $W(z)$ is the Lambert function (the solution of $z = W(z)\exp(W(z))$).

Regime	Range of validity	η	ζ	$b(0)$
1	$\Theta^5 \ll \Lambda \ll \Theta$	$\Lambda^{1/4}\Theta^{3/4}$	$\Lambda^{-1/2}\Theta^{1/2}$	$\Lambda^{1/4}\Theta^{-1/4}$
2	$\Lambda \ll 1$, $\Lambda \ll \Theta^5$	$\Lambda^{2/5}$	$\Lambda^{-2/5}$	$\Lambda^{1/5}$
3	$1 \ll \Lambda \ll \Theta(\log\Theta)^2$	$2\,W(\Lambda^{1/2}/2)$	1	1
4	$1 \ll \Theta$, $\Theta(\log\Theta)^2 \ll \Lambda$	$\log\Theta$	1	1
5	$\Theta \ll 1$, $\Theta \ll \Lambda$	Θ	1	1

where δ is the characteristic length scale over which $\sigma(x)$ decays, and $g(y)$ is some decaying function of y that is independent of any parameters. Then

$$\begin{aligned} K_c &= 2\left(\frac{L}{\pi}\right)^{1/2}\int_0^L \frac{\sigma(0)g(x/\delta)}{(L^2-x^2)^{1/2}}dx \\ &= \sigma(0)\delta^{1/2}\cdot 2\left(\frac{\rho}{\pi}\right)^{1/2}\int_0^\rho \frac{g(y)}{(\rho^2-y^2)^{1/2}}dy \\ &= \sigma(0)\delta^{1/2}f(\rho) \end{aligned} \tag{70}$$

where $\rho = L/\delta$. The dynamical hypothesis that v is maximal implies that ρ must be an extremum for $f(\rho)$. Let $\rho = \rho_c$ be this extremum, with $f(\rho_c) = f_c$ its extreme value. Since $f(\rho)$ is assumed not to depend on any of the parameters in the problem, ρ_c and f_c will simply be some order 1 numbers. Thus Yakobson's approach leads to

$$L = \rho_c\delta, \tag{71}$$

$$K_c = f_c\sigma(0)\delta^{1/2}, \tag{72}$$

which is exactly the same as the simplified criterion used here up to order 1 constants. In detail, Yakobson's particular problem has

$$g(y) = e^{-y}, \tag{73}$$

$$f(y) = \sqrt{\pi y}(I_0(y) - L_0(y)), \tag{74}$$

$$\rho_c = 0.917291, \tag{75}$$

$$f_c = 0.986713, \tag{76}$$

where I_0 is the zeroth order modified Bessel function of the first kind, and L_0 is the zeroth order modified Struve function.

Yakobson's (1991) concentration problem is the following

$$-v\frac{dc}{dx} = D\frac{d^2c}{dx^2}. \tag{77}$$

with boundary conditions

$$D\frac{dc}{dx}(0) = k_e c(0), \quad c(\infty) = c_\infty, \tag{78}$$

where k_e is an evaporation constant. The stress is related through

$$\sigma(x) = \beta E(1 - c(x)/c_\infty). \tag{79}$$

There is just one non-dimensional parameter in this problem, namely

$$\Delta = \frac{k_e}{D}\left(\frac{K_c}{\beta E}\right)^2. \tag{80}$$

As before, non-dimensional variables can be introduced as

$$\eta = \frac{v}{D}\left(\frac{K_c}{\beta E}\right)^2, \quad \zeta = L\left(\frac{\beta E}{K_c}\right)^2, \tag{81}$$

$$\mu = \frac{k_e}{v} = \frac{\Delta}{\eta}, \quad \lambda = \frac{Lv}{D} = \eta\zeta. \tag{82}$$

Non-dimensionally ($x' = xv/D$), the concentration field is

$$1 - c'(x') = \frac{e^{-x'}}{1+\mu^{-1}}. \tag{83}$$

Thus

$$\lambda = 1, \quad 1-c'(0) = \frac{1}{1+\mu^{-1}}. \tag{84}$$

The non-dimensional fracture criterion is

$$1 = \zeta^{1/2}(1-c'(0)), \tag{85}$$

and the relationships in Eq. (82) imply

$$\eta\left(1+\frac{\eta}{\Delta}\right)^2 = 1, \tag{86}$$

$$\zeta = \eta^{-1}. \tag{87}$$

There are two asymptotic regimes. If $\Delta \gg 1$ ("brittle fracturing") then

$$\eta = 1, \quad v = D\left(\frac{\beta E}{K_c}\right)^2, \tag{88}$$

$$\zeta = 1, \quad L = \left(\frac{K_c}{\beta E}\right)^2, \tag{89}$$

which is similar to regimes 4 and 5 in the reaction–diffusion model. If $\Delta \ll 1$ ("evaporation controlled")

$$\eta = \Delta^{2/3}, \quad v = D^{1/3}\left(\frac{\beta E k_e}{K_c}\right)^{2/3} \tag{90}$$

$$\zeta = \Delta^{-2/3}, \quad L = \left(\frac{DK_c}{\beta E k_e}\right)^{2/3}, \tag{91}$$

which is similar in form to regime 2 in the reaction–diffusion model. The scalings above are also seen in more sophisticated models, such as those by Boeck et al. (1999) and Malthe-Sørenssen et al. (2006).

D.2. Spheroidal weathering: Fletcher et al. (2006)

Fletcher et al. (2006) have also developed a model that couples a reaction–diffusion equation to a fracture mechanics problem to study chemical weathering. In fact, their model is very closely related to that considered here. Table 4 provides a mapping between the notation used by (Fletcher et al., 2006) and that used here. Their reaction–diffusion problem has the slight difference that their reaction rate $\propto w^{1/4}a$ with a cut-off for low concentrations, rather than reaction rate $\propto wa$ used here. The fracture mechanics is also treated a little differently: Fracturing is considered as an episodic process that occurs when the integrated elastic strain energy reaches a threshold value given by the surface energy of fracture. After each fracturing event the front moves forward to the cut-off point for the reaction. Thus the length scale for fracturing (crack spacing) in the (Fletcher et al., 2006) model is also set by the length scale over which a concentration profile decays, but it is the concentration profile of the water w rather than that of the product b which is used. In regimes 1, 2, and 5 the length scales for decay of product b and water w are the same, but in regimes 3 and 4 they are different, and in those regimes differences between our model and that of Fletcher et al. (2006) are expected.

Table 4
A mapping between the notation used here and that of Fletcher et al. (2006). The value of α quoted ($\alpha = 1.26\times10^{-7}$) differs from that directly quoted by Fletcher et al. (2006) ($\alpha = 6.32\times10^{-9}$) due to typographical errors.

Our model	Fletcher et al. notation	Fletcher et al. value
E	E	10^{11} Pa
K_c	$\sqrt{\frac{2\Gamma E}{1-\nu}}$	7.30×10^{6} Pa m$^{1/2}$
β	$\frac{f_0}{3(1-\nu)}\frac{\Delta V}{V}$	1.11×10^{-3}
b_0	$\frac{f_0}{V_{FeO}}$	4170 mol m^{-3}
w_0	ϕc_R	2.3×10^{-3} mol m^{-3}
κ	$\rho MSkV_{FeO}$	1.12×10^{-10} s^{-1}
r	r	0.25
s	1	1
D	$\frac{D\phi^{m-1}}{\tau}$	1.67×10^{-8} m^2 s^{-1}
v	ω	3.18×10^{-12} m s^{-1}
L	W	0.026 m
Λ	α	1.26×10^{-7}
Θ	$\frac{\alpha}{\Lambda}$	2.20×10^{-6}

A connection can be made with the simplified fracture criterion used here. The energy fracture criterion used by Fletcher et al. (2006) is

$$\int_0^L U(x)dx = 2\Gamma, \tag{92}$$

where Γ is the surface energy of fracture, and $U(x)$ is the elastic energy density. $U(x)$ is given by

$$U(x) = \frac{\sigma^2(x)}{E}. \tag{93}$$

There will also be a dependence on Poisson's ratio ν, but this depends on the specific details of the elastic problem, and has been neglected here. The surface energy of fracture can be related to the fracture toughness by

$$2\Gamma = \frac{K_c^2}{E}, \tag{94}$$

Again the ν dependence has been neglected. Thus the fracture criterion is

$$\int_0^L \sigma^2(x)dx = K_c^2. \tag{95}$$

Writing $\sigma(x) = \sigma(0)g(x/\delta)$ as in Eq. (69) yields

$$K_c = \mu_c \sigma(0)\delta^{1/2}, \tag{96}$$

where μ_c is

$$\mu_c = \left(\int_0^{L/\delta} g^2(y)dy\right)^{1/2}, \tag{97}$$

If the length scales for decay of the product b and water w are the same, then $L = \delta$, and μ_c is simply some order 1 constant. Thus the two fracturing criteria are equivalent in this case.

The two non-dimensional groups considered by Fletcher et al. (2006) can be related to those used here by

$$\Lambda_F = \frac{\Lambda}{\Theta}, \quad \alpha_F = \Lambda, \tag{98}$$

where subscript F refers to (Fletcher et al.'s, 2006) notation. Their numerics used $\Lambda_F = 0.0572$ and $\alpha_F = 1.26\times10^{-7}$ ($\Lambda = 1.26\times10^{-7}$ and $\Theta = 2.20\times10^{-6}$), which suggests they should be in regime 1. By conducting numerical simulations of their time-dependent problem they found that a steady state is reached, with the front propagating at a constant velocity. Their distance between fractures is given by ((18) of Fletcher et al. (2006))

$$W_F \approx 1.44 x_F^\star \Lambda_F^{-1/2} = 1.44\left(\frac{K_c}{\beta E}\right)^2 \Lambda^{-1/2}\Theta^{1/2}, \tag{99}$$

which is the same scaling as regime 1,

$$L = \left(\frac{K_c}{\beta E}\right)^2 \Lambda^{-1/2}\Theta^{1/2}. \quad (100)$$

Their weathering advance rate $\omega_F = W_F/t_{Fcrack}$ ((22) of Fletcher et al. (2006)) is

$$\omega_F = 0.660\frac{x_F^\star}{t_F^\star}\Lambda_F^{-4/5}\alpha_F = 0.660D\left(\frac{\beta E}{K_c}\right)^2\Lambda^{1/5}\Theta^{4/5} \quad (101)$$

which is almost, but not quite, the same scaling as regime 1,

$$v = D\left(\frac{\beta E}{K_c}\right)^2\Lambda^{1/4}\Theta^{3/4}. \quad (102)$$

The difference in the scalings is in the powers of Λ and Θ, which are 0.25 and 0.75 in the analysis here, but 0.2 and 0.8 for Fletcher et al. (2006). However, this difference might be explained by the fact that Fletcher et al.'s (2006) scalings are based on best fits to their numerical simulations rather than rigorous asymptotic analysis. If the same scalings were to hold, the corrected version of Eq. (22) of Fletcher et al. (2006) would be

$$\omega_F = 0.764\frac{x_F^\star}{t_F^\star}\Lambda_F^{-3/4}\alpha_F, \quad (103)$$

i.e. a coefficient of -0.75 rather than -0.8 for Λ_F. Written out in full, Fletcher et al.'s (2006) expressions relating crack length and weathering advance rate would become (in their notation)

$$W = 1.44\left(\frac{D\phi^m c_R}{r\tau\rho MSkf_0}\right)^{1/2}, \quad (104)$$

$$\omega = 0.764(\rho MSk)^{1/4}\left(\frac{D\phi^m c_R}{r\tau f_0}\right)^{3/4}\left[\frac{E\left(\frac{f_0}{3}\frac{\Delta V}{V}\right)^2}{2\Gamma(1-\nu)}\right]^{1/2} V_{FeO}. \quad (105)$$

References

Aharonov, E., Tenthorey, E., Scholz, C.H., 1998. Precipitation sealing and diagensis 2. Theoretical analysis. J. Geophys. Res. 103, 23969–23981. doi:10.1029/98JB02230.

Akbulut, M., Piskin, O., Karayigit, A.I., 2006. The genesis of the carbonatized and silicified ultramafics known as listvenites: a case study from the Mihaliccik region (Eskisehir), NW Turkey. Geol. J. 41, 557–580. doi:10.1002/gj.1058.

Alt, J.C., Teagle, D.A.H., 1999. The uptake of carbon during alteration of oceanic crust. Geochim. Cosmochim. Acta 63, 1527–1535. doi:10.1016/S0016-7037(99)00123-4.

Andreani, M., Luquot, L., Gouze, P., Godard, M., Hois, E., Gibert, B., 2009. Experimental study of carbon sequestration reactions controlled by the percolation of CO_2-rich brine through peridotites. Environ. Sci. Technol. 43, 1226–1231. doi:10.1021/es8018429.

Auclair, M., Gauthier, M., Trottier, J., Jébrak, M., Chartrand, F., 1993. Mineralogy, geochemistry, and paragenesis of the Eastern Metals serpentinite-associated Ni–Cu–Zn deposit, Quebec Appalachians. Econ. Geol. 88, 123–138. doi:10.2113/gsecongeo.88.1.123.

Bach, W., Garrido, C.-J., Paulick, H., Harvey, J., Rosner, M., Party, S.S., 2004. Seawater–peridotite interactions: first insights from ODP Leg 209, MAR 15°N. Geochem. Geophys. Geosyst. 5, Q09F26. doi:10.1029/2004GC000744.

Barnes, I., O'Neil, J.R., 1969. Relationship between fluids in some fresh alpine-type ultramafics and possible modern serpentinization, western United States. GSA Bull. 80, 1947–1960. doi:10.1130/0016-7606(1969) 80[1947:TRBFIS]2.0.CO;2.

Barnes, I., LaMarche, V.C., Himmelberg, G., 1967. Geochemical evidence of present-day serpentinization. Science 156, 830–832. doi:10.1126/science.156.3776.830.

Bartetzko, A., 2005. Effect of hydrothermal ridge flank alteration on the in situ physical properties of oceanic crust. J. Geophys. Res. 110, B06203. doi:10.1029/2004JB003228.

Becker, K., Davies, E., 2003. New evidence for age variation and scale effects of permeabilities of young oceanic crust from borehole thermal and pressure measurements. Earth Planet. Sci. Lett. 210, 499–508. doi:10.1016/S0012-821X(03)00160-2.

Boeck, T., Bahr, H.A., Lampenscherf, S., Bahr, U., 1999. Self-driven propagation of crack arrays: a stationary two-dimensional model. Phys. Rev. E 59, 1408–1416. doi:10.1103/PhysRevE.59.1408.

Brace, W.F., 1977. Permeability from resistivity and pore shape. Geophys. Res. Lett. 82, 3343–3349.

Bruni, J., Canepa, M., Chiodini, G., Cioni, R., Cipolli, F., Longinelli, A., Marini, L., Ottonello, G., Zuccolini, M.V., 2002. Irreversible water–rock mass transfer accompanying the generation of the neutral, $MgHCO_3$ and high-pH, CaOH spring waters of the Genova province, Italy. Appl. Geochem. 17, 455–474. doi:10.1016/S0883-2927(01)00113-5.

Chizmeshya, A.V.G., McKelvy, M.J., Squires, K., Carpenter, R.W., Béarat, H., 2007. DOE Final Report 924162. A novel approach to mineral carbonation: Enhancing carbonation while avoiding mineral pretreatment process cost. Tech. rep., Tempe, AZ, Arizona State University.

Correns, C.W., 1949. Growth and dissolution of crystals under linear pressure. Discuss. Faraday Soc. 5, 267–271.

Correns, C.W., Steinborn, W., 1939. Experimente zur messung and erklärung der sogenannten kristallisationskraft. Zeit. Krist. 101, 117–133.

Farver, J.R., Yund, R.A., 1991. Measurement of oxygen grain boundary diffusion in natural, fine-grained, quartz aggregates. Geochim. Cosmochim. Acta 55, 1597–1607. doi:10.1016/0016-7037(91)90131-N.

Farver, J.R., Yund, R.A., 1992. Oxygen diffusion in a fine-grained quartz aggregate with wetted and non-wetted microstructures. J. Geophys. Res. 97, 14017–14029. doi:10.1029/92JB01206.

Flatt, R.J., Steiger, M., Scherer, G.W., 2007. A commented translation of the paper by C. W. Correns and W. Steinborn on crystallization pressure. Environ. Geol. 52, 187–203. doi:10.1007/s00254-006-0509-5.

Fletcher, R., Buss, H., Brantley, S., 2006. A spheroidal weathering model coupling porewater chemistry to soil thicknesses during steady-state denudation. Earth Planet. Sci. Lett. 244, 444–457. doi:10.1016/j.epsl.2006.01.055.

Hansen, L.D., Dipple, G.M., Gordon, T.M., Kellet, D.A., 2005. Carbonated serpentinite (listwanite) at Atlin, British Columbia: A geological analogue to carbon dioxide sequestration. Can. Mineral. 43, 225–239. doi:10.2113/gscanmin.43.1.225.

Iyer, K., Jamtveit, B., Mathiesen, J., Malthe-Sørenssen, A., Feder, J., 2008. Reaction-assisted hierarchical fracturing during serpentinization. Earth Planet. Sci. Lett. 267, 503–516. doi:10.1016/j.epsl.2007.11.060.

Jamtveit, B., Malthe-Sørenssen, A., Kostenko, O., 2008. Reaction enhanced permeability during retrogressive metamorphism. Earth Planet. Sci. Lett. 267, 620–627. doi:10.1016/j.epsl.2007.12.016.

Jamtveit, B., Putnis, C.V., Malthe-Sørenssen, A., 2009. Reaction induced fracturing during replacement processes. Contrib. Mineral. Petrol. 157, 127–133. doi:10.1007/s00410-008-0324-y.

Kelemen, P.B., Matter, J.M., 2008. In situ carbonation of peridotite for CO_2 storage. Proc. Natl Acad. Sci. USA 105, 17295–17300. doi:10.1073/pnas.0805794105.

Kelemen, P.B., Kikawa, E., Miller, D.J., 2004. Proc. ODP, Init. Repts. 209. Tech. rep., College Station, TX, Ocean Drilling Program. doi:10.2973/odp.proc.ir.209.101.2004.

Kelemen, P.B., Kikawa, E., Miller, D.J., Party, S.S., 2007. Processes in a 20-km-thick conductive boundary layer beneath the Mid-Atlantic Ridge, 14°–16°N. Proc. ODP, Sci. Results, 209. College Station, TX, Ocean Drilling Program, pp. 1–33. doi:10.2973/odp.proc.sr.209.001.2007.

MacDonald, A.H., Fyfe, W.S., 1985. Rate of serpentinization in sea-floor environments. Tectonophys 116, 123–135. doi:10.1016/0040-1951(85)90225-2.

Madu, B.E., Nesbitt, B.E., Muehlenbachs, K., 1990. A mesothermal gold–stibnite–quartz vein occurrence in the Canadian Cordillera. Econ. Geol. 85, 1260–1268. doi:10.2113/gsecongeo.85.6.1260.

Malthe-Sørenssen, A., Jamtveit, B., Meakin, P., 2006. Fracture patterns generated by diffusion controlled volume changing reactions. Phys. Rev. Lett. 96, 245501. doi:10.1103/PhysRevLett.96.245501.

Martin, B., Fyfe, W.S., 1970. Some experimental and theoretical observations on the kinetics of hydration reactions with particular reference to serpentinization. Chem. Geol. 6, 185–202. doi:10.1016/0009-2541(70)90018-5.

Milsch, H., Seibt, A., Spangenberg, E., 2009. Long-term petrophysical investigations on geothermal reservoir rocks at simulated in situ conditions. Transp. Porous Med. 77, 59–78. doi:10.1007/s11242-008-9261-5.

Morrow, C., Moore, D., Lockner, D., 2001. Permeability reduction in granite under hydrothermal conditions. J. Geophys. Res. 106, 30551–30560. doi:10.1029/2000JB000010.

Naldrett, A.J., 1966. Talc–carbonate alteration of some serpentinized ultramafic rocks south of Timmins, Ontario. J. Petrol. 7, 489–499.

Nasir, S., Al Sayigh, A.R., Al Harthy, A., Al-Khirbash, S., Al-Jaaidi, O., Musllam, A., Al-Mishwat, A., Al-Bu'saidi, S., 2007. Mineralogical and geochemical characterization of listwaenite from the Semail ophiolite, Oman. Chemie Der Erde Geochem. 67, 213–228. doi:10.1016/j.chemer.2005.01.003.

Neal, C., Stanger, G., 1985. Past and present serpentinization of ultramafic rocks: an example from the Semail ophiolite nappe of northern Oman. The Chemistry of Weathering. D. Reidel Publishing Company, Holland, pp. 249–275.

O'Connor, W., Dahlin, D., Rush, G., Gerdemann, S., Penner, L., Nilsen, D., 2005. Final report: aqueous mineral carbonation. Mineral availability, pretreatment, reaction parametrics, and process studies, Report DOE/ARC-TR-04-002. Tech. rep., Office of Process Development, Albany Research Center, Office of Fossil Energy, US DOE, Albany, OR.

Paulick, H., Bach, W., Godard, M., Hoog, J.C.M.D., Suhr, G., Harvey, J., 2006. Geochemistry of abyssal peridotites (Mid-Atlantic Ridge, 15°20′N, ODP Leg 209): implications for fluid/rock interaction in slow spreading environments. Chem. Geol. 234, 179–210. doi:10.1016/j.chemgeo.2006.04.011.

Poupeau, G., Saddiqi, O., Michard, A., Goffé, B., Oberhänsli, R., 1998. Late thermal evolution of the Oman Mountains subophiolitic windows: apatite fission-track thermochronology. Geology 26, 1139–1142. doi:10.1130/0091-7613(1998)026<1139;LTEOTO>l2.3CO;2.

Rijniers, L.A., Huinink, L.P., Kopinga, K., 2005. Experimental evidence of crystallization pressure inside porous media. Phys. Rev. Lett. 94, 075503. doi:10.1103/PhysRevLett.94.075503.

Robinson, P.T., Malpas, J., Zhou, M.F., Ash, C., Yang, J.S., Bai, W.J., 2005. Geochemistry and origin of listwaenites in the Sartohay and Luobnsa ophiolites, China. Int. Geol. Rev. 47, 177–202.

Røyne, A., Jamtveit, B., Mathiesen, J., Malthe-Sørenssen, A., 2008. Controls on rock weathering rates by reaction-induced hierarchical fracturing. Earth Planet. Sci. Lett. 275, 364–369. doi:10.1016/j.epsl.2008.08.035.

Santti, J., Kontinen, A., Sorjonen-Ward, P., Johanson, B., Pakkanen, L., 2006. Metamorphism and chromite in serpentinized and carbinate-silica-altered peridotites of the Paleoproterozoic Outokumpu-Jormua Ophiolite Belt, Eastern Finland. Int. Geol. Rev. 48, 494–546.

Schandl, E.S., Naldrett, A.J., 1992. CO_2 metasomatism of serpentinites south of Timmins, Ontario. Can. Mineral. 30, 93–108.

Schandl, E.S., Wicks, F.J., 1993. Carbonate and associated alteration of ultramafic and rhyolitic rocks at the Hemingway Property, Kidd Creek Volcanic Complex, Timmins, Ontario. Econ. Geol. 88, 1615–1635. doi:10.2113/gsecongeo.88.6.1615.

Scherer, G.W., 1999. Crystallization in pores. Cem. Concr. Res. 29, 1347–1358. doi:10.1016/S0008-8846(99)00002-2.

Scherer, G.W., 2004. Stress from crystallization of salt. Cem. Concr. Res. 34, 1613–1624. doi:10.1016/j.cemconres.2003.12.034.

Schramm, B., Devey, C., Gillis, K.M., Lackschewitz, K., 2005. Quantitative assessment of chemical and mineralogical changes due to progressive low-temperature alteration of East Pacific Rise basalts from 0 to 9 Ma. Chem. Geol. 218, 281–313. doi:10.1016/j.chemgeo.2005.01.011.

Sprunt, E.S., Brace, W.F., 1974. Direct observations of microcavities in crystalline rocks. Int. J. Rock Mech. Min. Sci. Geomech. Abstr. 11, 139–150. doi:10.1016/0148-9062(74)92874-5.

Stanger, G., 1985. Silicified serpentinite in the Semail nappe of Oman. Lithos 18, 13–22. doi:10.1016/0024-4937(85)90003-9.

Tenthorey, E., Scholz, C.H., Aharonov, E., Léger, A., 1998. Precipitation scaling and diagensis 1. Experimental results. J. Geophys. Res. 103, 23951–23967. doi:10.1029/98JB02229.

Ucurum, A., 2000. Listwaenites in Turkey: perspectives on formation and precious metal concentration with reference to occurrences in East-Central Anatolia. Ofioliti 25, 15–29.

Ucurum, A., Larson, L.T., 1999. Geology, base-precious metal concentration and genesis of the silica-carbonate alteration (listwaenties) from late Cretaceous ophiolitic melanges at central east Turkey. Chem. Erde 59, 77–104.

Walder, J., Hallet, B., 1985. A theoretical model of the fracture of rock during freezing. Geol. Soc. Am. Bull. 96, 336–346. doi:10.1130/0016-7606(1985)96<336:ATMOTF>2.0.CO;2.

Wilde, A., Simpson, L., Hanna, S., 2002. Preliminary study of Cenozoic alteration and platinum deposition in the Oman ophiolite. J. Virtual Explorer 6, 7–13.

Wong, T.-F., Fredrich, J.T., Gwanmesia, G.D., 1989. Crack aperture statistics and pore space fractal geometry of Westerley Granite and Rutland Quartzite: Implications for an elastic model of rock compressibility. J. Geophys. Res. 94, 10267–10278.

Wu, Y.-S., Zhang, K., Liu, H.-H., 2006. Estimating large-scale fracture permeability of unsaturated rock using barometric pressure data. Vadose Zone J. 5, 1129–1142. doi:10.2136/vzj2006.0015.

Wu, Y.-S., Ye, M., Sudicky, E.A., 2010. Fracture-flow-enhanced matrix diffusion in solute. Transp. Porous Med. 81, 21–34. doi:10.1007/s11242-009-9383-4.

Yakobson, B.I., 1991. Morphology and rate of fracture in chemical decomposition of solids. Phys. Rev. Lett. 67, 1590–1593. doi:10.1103/PhysRevLett.67.1590.

Yund, R.A., 1997. Rates of grain boundary diffusion through enstatite and forsterite reaction rims. Contrib. Mineral. Petrol 126, 224–236. doi:10.1007/s004100050246.